Inorg. Chim. Acta., 7, 365 (1973).
7. B. S. Furniss, A. J. Hannaford, P. W. G. Smith, and A. R. Tatchell, "Vogel's Textbook of Practical Organic Chemistry", 5th ed., Long-man, London, p. 983, 1988.
8. D. D. Perrin and W. L. Armarego, "Purification of Laboratory Chemicals", 3rd ed., Pergamon Press, Oxford, 1988.
9. J. Basset, R. C. Denney, G. H. Jeffey, and J. Mendharn, "Vogel's Textbook of Quantitative Inorganic Analysis", 4th ed., Longman, New York, U.S.A., p. 471, 1978/
10. W. J. Geary, *Coord. Chem. Rev.*, 7, 81 (1971).
11. N. N. Greenwood, B. P. Straughan, and A. E. Wilson, *J. Chem. Soc., A*, 2209 (1968).
12. (a) P. C. H. Mitchel, *Coord. Chem. Rev.*, **1**, 315 (1966); (b) M. Chaudhury, *Inorg. Chem.*, **24**, 3011 (1985).
13. (a) W. E. Hill, N. Atabay, C. A. McAuliffe, F. P. McCullough, and S. M. Razzolci, *Inorg. Chim. Acta.*, **35**, 35 (1979); (b) S. Chandra and K. K. Sharma, *Transition Met. Chem.*, **9**, 1 (1984).
14. K. Nakamoto, "Infrared Spectra of Inorganic and Coordination Compounds", 2nd ed., John Wiley and Sons, New York, p. 187, 1970.
15. A. Sabatini and I. Bertini, *Inorg. Chem.*, **4**, 959 (1965).
16. K. Biemann, "Tables of Spectral Data for structure Determination of Organic Compounds", 2nd ed., Spring-Verlag, New York, 1989.
17. (a) S. Purohit, A. P. Kolay, L. S. Prasad, P. T. Manoharan, and S. Ghosh, *Inorg. Chem.*, **28**, 3735 (1989); (b) A. Symal and M. A. Bari Niazi, *Transition Met. Chem.*, **10**, 54 (1985).
18. (a) M. Chaudhury, *J. Chem. Soc. Dalton Trans.*, 115 (1984); (b) F. W. Moore and R. E. Rice, *Inorg. Chem.*, 7, 2511 (1968).
19. A. Marchi, A. Duatti, R. Rossi, L. Magon, R. Pasqualini, V. Bertolasi, V. Ferretti, and G. Gilli, *J. Chem. Soc. Dalton Trans.*, 1743 (1988).
20. S. J. Lippard, "Progress in Inorganic Chemistry", 1st ed., John Wiley and Sons, New York, U.S.A., Vol. 22, p. 57, 1977.

Kinetics and Mechanisms of the Oxidation of Carbon Monoxide on $Eu_{1-x}Sr_xCoO_{3-y}$ Perovskite Catalysts

Dong Hoon Lee, Joon Ho Jang, Hong Seok Kim, Yoo Young Kim, Jae Shi Choi, and Keu Hong Kim*

Department of Chemistry, Yonsei University, Seoul 120-749. *Received March 23, 1992*

The catalytic oxidation of CO on perovskite $Eu_{1-x}Sr_xCoO_{3-y}$ has been investigated at reaction temperatures from 100 to 250℃ under stoichiometric CO and O_2 partial pressures. The microstructure and Sr-substitution site of the catalyst were studied by means of infrared spectroscopy. The reaction rates were found to be correlated with 1.5- and 1.0- order kinetics with and without a CO_2 trap, respectively; first- and 0.5-order with respect to CO and 0.5-order to O_2 with the activation energy of 0.37 eV mol^{-1}. It was found from IR, σ and kinetic data that O_2 adsorbs as an ionic species on the oxygen vacancies, while CO adsorbs on the lattice oxygens. The oxidation reaction mechanism is suggested from the agreement between IR, σ and kinetic data.

Introduction

Most metal oxides contain an excess oxygen or excess metal in their crystal structures. The catalytic activity of nickel oxide is due to excess oxygen[1] while that of zinc oxide is due to oxygen vacancies formed by the excess zinc metal.[2-4] The positive holes caused by the excess oxygen activate the reactant molecules and the anion vacancies due to the excess metal are responsible for the catalytic activity.[5,6] On the other hand, the catalytic activity of metal oxides on the oxidation of carbon monoxide varies with the amount of impurity doped in the oxide catalyst inducing the positive holes or anion vacancies.[7-9] The bulk structure of perovskite-type mixed oxide has been well characterized and the formations of oxygen vacancies and metal deficiencies are easily controlled by the incorporation of the foreign atoms without changing the fundamental structure.[10]

In this point of view, the perovskite-type $EuCoO_3$ doped with Sr was selected, since the Sr doping may play an important role in the enhancement of the catalytic activity. We prepared $Eu_{1-x}Sr_xCoO_{3-y}$ catalysts with different atomic mole fraction of Sr and characterized them by X-ray diffraction analysis and infrared spectroscopy.

Experimental

Catalyst Preparation. The $Eu_{1-x}Sr_xCoO_{3-y}$ powder was prepared by mixing appropriate weights of Eu_2O_3 (99.99%), $SrCO_3$ (99.995%) and CoO from Co_3O_4 (99.995%) powders all obtained from the Aldrich Co. in ethanol, stirring them for 96h to obtain a homogeneous dispersed powders, filtering and drying at 150℃, putting in a covered Pt crucible, firing in air at 1150℃ for 96h, and then slowly cooling to room temperature. The sample powder was ball-milled for 3h, cal-

cined at 950℃ for 96h, and then cooled rapidly to room temperature. The $Eu_{1-x}Sr_xCoO_{3-y}$ pellet was prepared by compressing some of the powder prepared by the above procedure under a pressure of 19.6 MPa into a pellet and sintering at 500℃ for 3h. The pellet was given a light abrasive polish onto surfaces, and then cut into a rectangular shape with suitable dimensions for measurement of electrical conductivity. The reactant gases CO and O_2 were prepared by the following procedure. The chemical reaction of $CaCO_3$ and Zn powders in mole ratio of 1 : 2 was performed by heating both materials at about 800℃ in quartz chamber connected to CO storage. The decomposition of potassium chlorate was carried out at 630℃. The CO and O_2 gases were purified by passing them over $CaCl_2$, P_2O_5, and glass wool. This was found to give CO and O_2 free from catalytic poisons by the test reaction of catalytic activity.

Structure and Microstructure. Powder X-ray diffraction was performed on a diffractometer (Philips, PW 1710, CuKα) equiped with a curved graphite monochromator in a selected beam path. The crystal structure was deduced from the diffraction pattern. The accurate lattice parameter (a) for each catalyst was obtained in the same method as described in the previous papers[11-17] based on the indexation of powder X-ray diffraction data. The obtained lattice parameter ($a=5.242$ Å) of pure $EuCoO_3$ with orthorhombic structure agrees with the ASTM value ($a=5.249$ Å). The lattice parameters b and c of $EuCoO_3$ and $Eu_{0.75}Sr_{0.25}CoO_{3-y}$ are 5.371 and 7.470 and 5.524 and 7.866 Å with orthorhombic structure, respectively. The a-lattice parameter for various Sr-substituted catalysts were obtained from the same manner. The obtained lattice parameters are $a=5.528$ Å for $x=0.25$ with orthorhombic structure, $a=3.806$ Å for $x=0.50$, and $a=3.843$ Å for $x=0.75$ with cubic structure in $Eu_{1-x}Sr_xCoO_{3-y}$ catalysts. The lattice parameters increase slightly with increasing amount of Sr substituted on same crystal structure. In order to see the crystal growth and morphology, the SEM micrographs were obtained using scanning electron microscope (Hitachi S-510).

The infrared spectra of catalysts extracted from KBr pellets were recorded at room temperature using an infrared spectrometer (Digilab-Division FTS-80) in the wavenumber range of 400 to 1000 cm^{-1}.

EDX, Nonstoichiometry, Surface area, and Thermal Analyses. The compositions of $Eu_{1-x}Sr_xCoO_{3-y}$ sintered at 1150℃ for 96h have been analyzed by EDX (Energy Dispersive X-ray), and show Eu=60.59, Sr=0, Co=25.18, and O=19.82% for $x=0$. For Sr-substituted samples, the compositions (%) are Eu=49.50, Sr=8.51, Co=26.73, and O=20.26 for $x=0.25$, Eu=37.22, Sr=19.13, Co=26.27, and O=20.15 for $x=0.50$ and Eu=17.60, Sr=31.50, Co=29.75, and O=20.65 for $x=0.75$, respectively. Based on EDX data, the effective values of x are almost the same as the nominal values, increasing with increasing Sr-substitution. On the other hand, the value of y also increases with Sr-substitution, satisfying the nonstoichiometry, however, y decreases with continuous Sr-substitution up to $x=0.75$. This indicates that the nonstoichiometric composition of present catalyst depends on the amount of Sr-substitution. The surface area of each sample (100-160 mesh) was measured by a Blain test and the measured values increase with x values, showing 1.38 ($x=0$), 2.34 ($x=0.25$), 2.45 m^2/g ($x=0.50$), respectively,

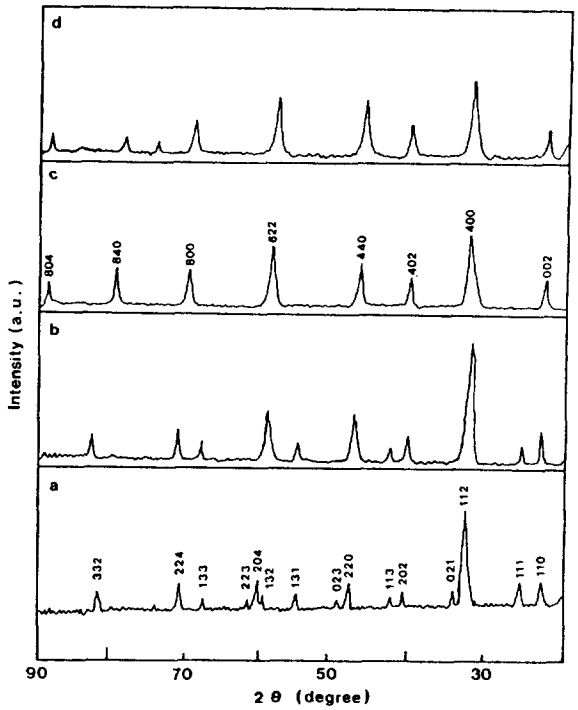

Figure 1. X-ray powder diffraction patterns of catalysts sintered at 1150℃ for 96 h. (a) $x=0$; (b) $x=0.25$; (c) $x=0.50$; (d) $x=0.75$ in $Eu_{1-x}Sr_xCoO_{3-y}$.

however the value decreases with further increasing Sr-substitution up to $x=0.75$ with 2.39 m^2/g. In order to confirm the phase transition, DTA and TGA measurments were carried out as a function of the amount of Sr in $Eu_{1-x}Sr_xCoO_{3-y}$ catalysts sintered at 1150℃. Both DTA and TGA show that the weight loss and phase change are not occured in the present Sr-substitution range.

Measurements of Electrical Conductivity. The electrical conductivity was measured in the temperatures from −73 to 250℃ under $P_{O_2}=0.2$ atm. The details of conductivity measurements have been described in the previous papers.[18-22] The conductivities were also measured at 250℃ under various P_{CO} and P_{O_2} in order to confirm the active sites of the catalyst. Prior to measurements, the catalysts were always pretreated with reactants for 40 min at 250℃ and then degassed for 1h at 500℃ and 1×10^{-3} torr.

Measurement of Reaction Rate. The catalytic oxidation reactions were carried out at 100-250℃ with 0.5-0.6 g of catalyst on the reaction chamber bed. This reaction chamber (142 ml) was connected to the high-vacuum system which contained CO and O_2 gas storage tanks, Baratron pressure gauge, gas chromatographs (molecular sieve, or Porapak Q), liquid nitrogen trap, electrical furnace, electrometers, potentiometers, lock-in amplifier, and small other instruments. The product (CO_2) was condensed by a liquid nitrogen trap and detected. The amounts of CO consumptions were evaluated from the measured CO_2 and pressure change, respectively. The product was also checked by CO_2 sensor (Thomas 5220) and a gas chromatograph.

Results and Discussion

Figure 1 shows the X-ray powder diffraction patterns of

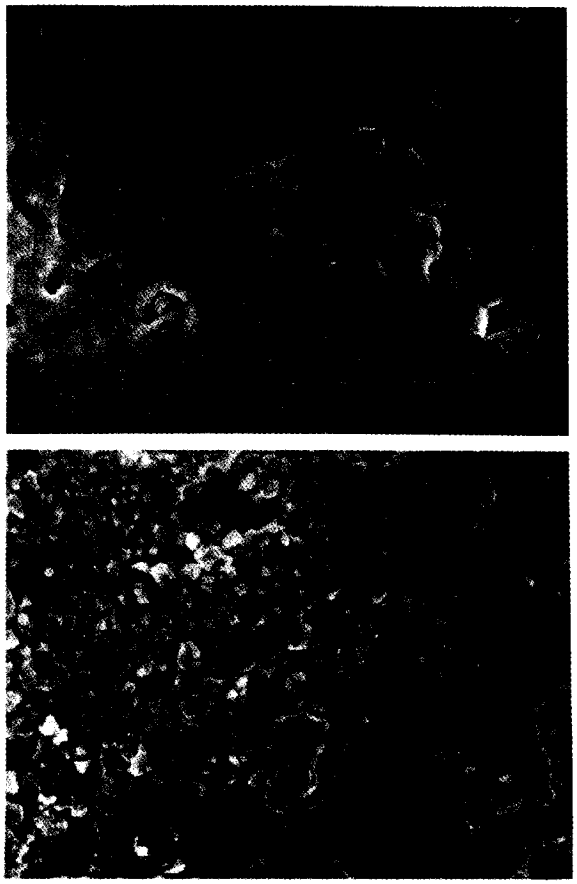

Figure 2. SEM micrographs for $Eu_{1-x}Sr_xCoO_{3-y}$ catalysts sintered at 1150℃; (a) $x=0.00$; (b) $x=0.25$.

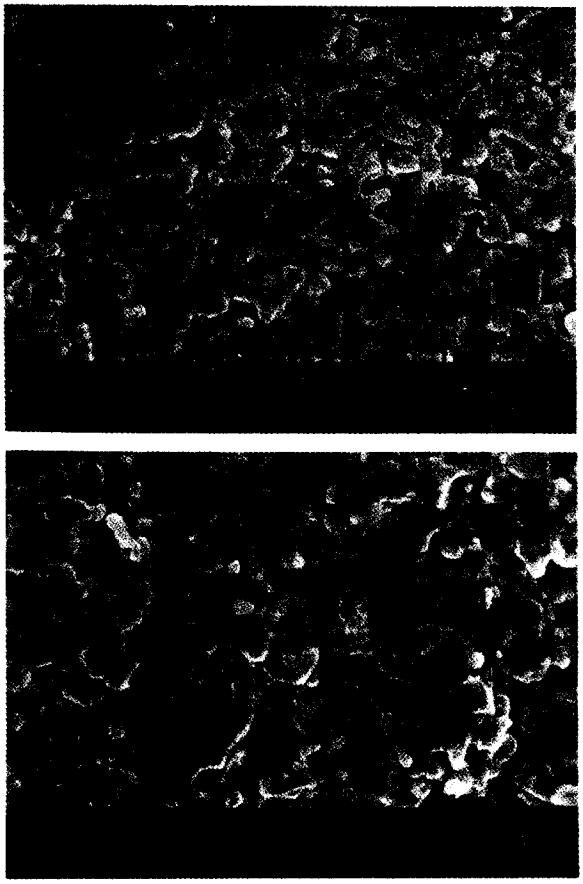

Figure 3. SEM micrographs for $Eu_{1-x}Sr_xCoO_{3-y}$ catalysts sintered at 1150℃; (a) $x=0.50$; (b) $x=0.75$.

specimens sintered at 1150℃ for 96h. As shown in Figure 1, no peaks corresponding to Eu_2O_3, SrO, and CoO appears and two series of peaks indicate two different structures. The peaks for (a) ($x=0$) and (b) ($x=0.25$) in Figure 1 are completely overlapped with those of orthorhombic $GdFeO_3$ on JCPDS file[23] and have same d values. On the other hand, the peaks for (c) ($x=0.50$) and (d) ($x=0.75$) show the same positions and intensities as those of cubic $SrCoO_3$ on JCPDS file[24] and same d values. As was mentioned in Experimental section, the lattice parameters obtained by Cohen method[25] increase with increasing Sr-substitution of both orthorhombic and cubic structures. This result can be explained by the fact that the ionic radius of Sr^{2+} (1.13 Å) is larger than that of Eu^{3+} (0.95 Å) so that the lattice parameter increases due to dopant addition. The increasing lattice parameter with increasing amount of Sr implies that the Sr is substituted for Eu in the solid solution region.[26] Following XRD data, no impurity phases are found in the present catalysts. Based on the DTA and TGA data, no phase transition occurs in the present range of Sr-substitution.

Figures 2 and 3 show the SEM micrographs for samples with $x=0$ and $x=0.25$, and $x=0.50$ and $x=0.75$, respectively. As can be seen in these Figures, the sizes of particles on surface are smaller from $x=0$ to $x=0.25$ and larger from $x=0.25$ up to $x=0.75$. On the other hand, the voids between surface particles are larger in size and number from $x=0$ to $x=0.25$ and smaller from $x=0.25$ up to $x=0.75$, re-

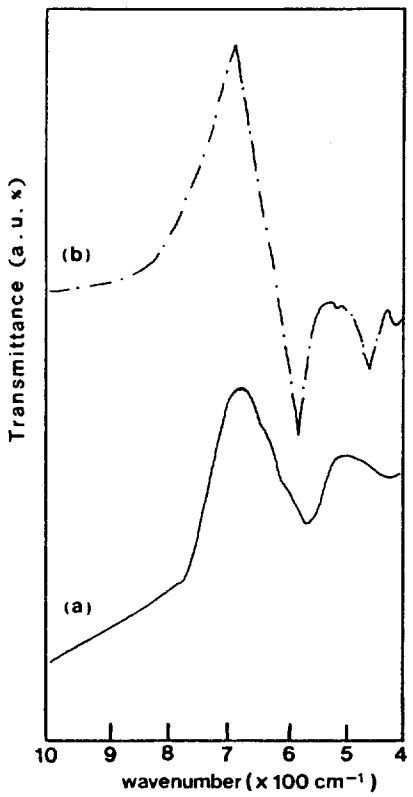

Figure 4. The infrared spectra of pure CoO (a) and $EuCoO_3$ (b).

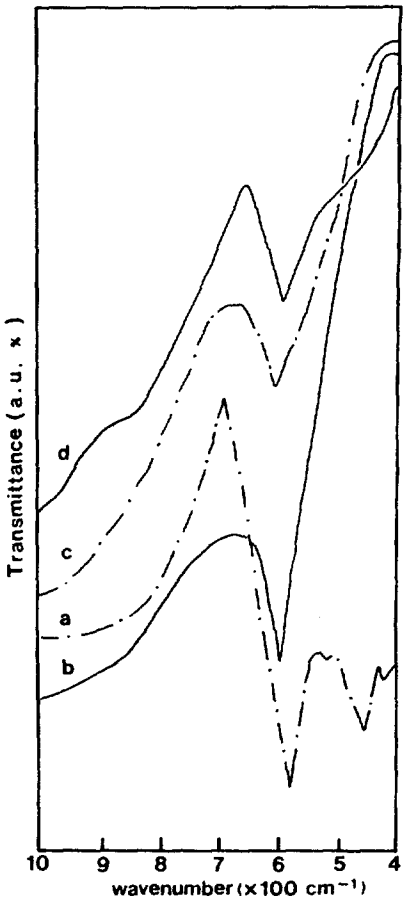

Figure 5. The infrared spectra of $Eu_{1-x}Sr_xCoO_{3-y}$ catalysts; (a) $x=0$; (b) $x=0.25$; (c) $x=0.50$; (d) $x=0.75$ in $Eu_{1-x}Sr_xCoO_{3-y}$.

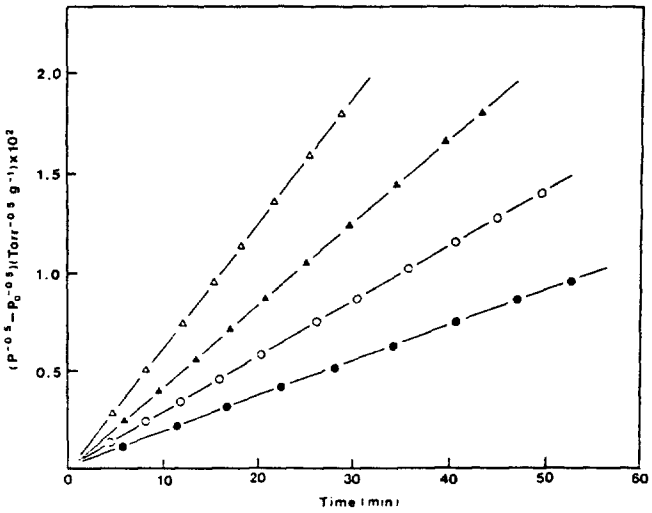

Figure 6. Rates of CO oxidation on $Eu_{0.5}Sr_{0.5}CoO_{3-y}$ at various temperatures. $P^\circ_{CO}=119$ torr; $P^\circ_{O_2}=58$ torr; catalyst=0.5g; surface area; 2.45 m^2/g; particle size : 100-160 mesh; P°, total initial pressure; P, total pressure; —●— (100℃); —○— (150℃); —▲— (200℃) and —△— (250℃).

Table 1. Temperature Dependence of Rate Constants (k, $torr^{-0.5}$, g^{-1}, min^{-1}) of the Oxidation of Carbom Monoxide on $Eu_{1-x}Sr_xCoO_{3-y}$ Catalysts

×	Temperature(℃)			
	100	150	200	250
0.25	2.12×10^{-6}	6.24×10^{-6}	1.19×10^{-5}	2.18×10^{-6}
0.50	9.27×10^{-5}	1.29×10^{-4}	2.09×10^{-4}	3.19×10^{-4}
0.75	1.98×10^{-6}	6.15×10^{-6}	1.08×10^{-5}	1.98×10^{-5}

spectively.

Figures 4(a) and 4(b) show the infrared spectra of pure CoO and $EuCoO_3$, respectively. In Figure 4(a), a single absorption band appears at 563 cm^{-1}, which is assigned to Co-O vibrations due to $Co^{3+}O_6$ in the cubic structure of CoO. However, in Figure 4(b), two absorption bands at 580 and 450 cm^{-1} are observed and considered to be due to the Co-O vibrations of $Co^{2+}O_4$ and $Co^{3+}O_6$ in the normal orthorhombic structure.

Figures 5(a), 5(b), 5(c), and 5(d) show the infrared spectra of $Eu_{1-x}Sr_xCoO_{3-y}$ for $x=0$ (a), $x=0.25$ (b), $x=0.50$ (c), and $x=0.75$ (d), respectively. As can be seen in Figures 5(b), 5(c) and 5(d), the vibrational bands due to Co-O are observed at 600, 610, and 590 cm^{-1} and conserved. These bands are shifted from 580 cm^{-1} ($x=0$) to 600 ($x=0.25$), 610 ($x=0.50$) and 590 cm^{-1} ($x=0.75$), implying that the bond nature of Co-O in $Eu_{1-x}Sr_xCoO_{3-y}$ is different from that in $EuCoO_3$. On the other hand, the 450 cm^{-1} band in $EuCoO_3$ is not observed in $Eu_{1-x}Sr_xCoO_{3-y}$ catalysts. The intensity of the 580 cm^{-1} band at $x=0$ is decreased as the amount of Sr incorporated in $Eu_{1-x}Sr_xCoO_{3-y}$ increases up to $x=0.50$ and then increases again from $x=0.5$ up to $x=0.75$. This indicates that the $x=0.50$, but decreases again from $x=0.5$ up to $x=0.75$ in $Eu_{1-x}Sr_xCoO_{3-y}$, confirming the increase and decrease of the nonstoichiometry. From the infrared spectra, it is known that the degree of nonstoichiometry depends on the concentration of oxygen atom which is bonded with Co atom.

The kinetic data are found to obey closely the expression $-dP/dt=kP_{CO+O_2}^{1.5}$ with respect to the total pressure in the reaction temperatures from 100 to 250℃. The total order was confirmed by the linearity as shown in Figure 6. The rate constants listed in Table 1 are found to be compatible with the Arrhenius equation, giving an activation energy of 0.37 eV·mol^{-1}. The oxidation rates, as shown in Table 2, were obtained from the variations of P_{CO} and P_{O_2} on the three different $Eu_{1-x}Sr_xCoO_{3-y}$ catalysts at 100 and 250℃, respectively. The exponents of the P_{CO} and P_{O_2} dependences are evaluated from the rate data in Table 2. The partial orders are found to be first for CO and half for O_2. The first and half orders imply that CO and O_2 may adsorb as a molecular and atomic ionic states, respectively.

The electrical conductivity (σ) increases with increasing temperature and amounts of Sr from $x=0$ to $x=0.50$ as shown in Figure 7. The magnitude of σ of $x=0.75$ is almost same as that of $x=0.25$. The temperature dependence of σ for $EuCoO_3$ is different from that for $Eu_{0.5}Sr_{0.5}CoO_{3-y}$, showing very small activation energy. The increasing conductivity with increasing amounts of Sr up to $x=0.75$ indicates that Sr substitution produces electrons into donor level by the disorder equilibrium, $O^{2-}=1/2\ O_2\ (g)+2e^-+V_o$ where O^{2-} is a lattice oxygen, e^- a donor electron and V_o an oxygen vacancy.

Table 2. Comparative Rates(r) of CO Oxidation as a Function of Partial Pressure of CO and O_2 on $Eu_{1-x}Sr_xCoO_{3-y}$ Catalysts

×	T(℃)	P_{CO}	P_{O_2}	r(torr, g^{-1}, min^{-1})
0.25	100	117	58	1.87×10^{-3}
	100	119	29	1.40×10^{-3}
	100	58	27	6.81×10^{-4}
	250	119	59	2.10×10^{-2}
	250	121	32	1.43×10^{-2}
	250	60	29	7.19×10^{-3}
0.50	100	119	57	8.59×10^{-2}
	100	118	28	5.86×10^{-2}
	100	61	32	2.99×10^{-2}
	250	119	59	3.01×10^{-1}
	250	121	31	2.14×10^{-1}
	250	62	29	1.16×10^{-1}
0.75	100	121	61	1.79×10^{-3}
	100	119	29	1.39×10^{-3}
	100	58	28	6.75×10^{-4}
	250	119	60	1.98×10^{-2}
	250	120	31	1.39×10^{-2}
	250	60	29	6.98×10^{-3}

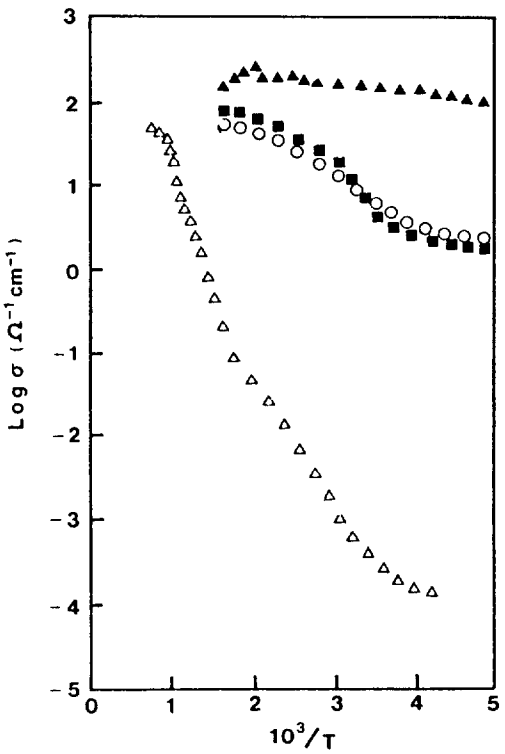

Figure 7. Log conductivity, vs. 1000/T at P_{O_2} of 0.2 atm for $EuCoO_3$ (△), $Eu_{0.75}Sr_{0.25}CoO_{3-y}$ (○), $Eu_{0.50}Sr_{0.50}CoO_{3-y}$ (▲) and $Eu_{0.25}Sr_{0.75}CoO_3$ (■) catalysts sintered at 1150℃.

Figure 8 shows the σ dependences on P_{CO} and P_{O_2} measured after equilibrium between catalyst and atmosphere. The σ increases with P_{CO}, but decreases with P_{O_2}. The magnitudes of σ are listed in Table 3 under various P_{CO} and P_{O_2} for $Eu_{0.5}Sr_{0.5}CoO_{3-y}$ catalyst. From the σ variation, it is known that the reactants can be chemisorbed on the catalyst surface. The charge transfer on the catalyst surface forms a double layer and is interpreted in terms of a space charge due to distributed ions. Actually, the mobile conduction electrons are associated with these charge transfers, but the density of energy levels at the band edge is so low that the conduction electrons are spreaded as a space charge. This space charge can affect the electrical properties of the present catalysts and their double layers can change the density of current carriers, controlling the electron concentration. The electron density at the catalyst surface will descrease due to the formation of double layers as a result of O_2 chemisorption on catalyst surface, showing decreases in σ with increasing P_{O_2}.

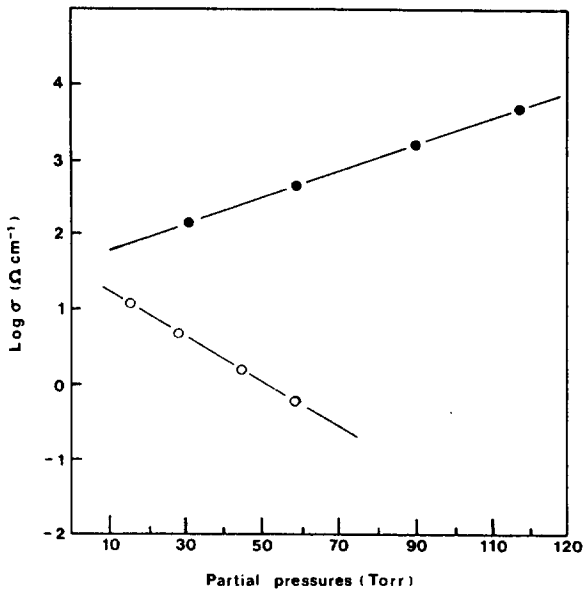

Figure 8. Electrical conductivities of $Eu_{0.50}Sr_{0.50}CoO_{3-y}$ catalyst under various P_{CO} —●— and P_{O_2} —○— at 250℃; pellet; sintered at 1150℃; equilibrium time : 1h.

Table 3. Electrical Conductivities of $Eu_{0.5}Sr_{0.5}CoO_{3-y}$ under Various Partial Pressure of CO and O_2 at 250℃

Reactants	Partial Pressures(torr)	σ(Ohm·cm)$^{-1}$
O_2	16	1.63×10^{1}
	29	5.49×10^{0}
	43	1.67×10^{0}
	59	5.93×10^{-1}
CO	31	1.69×10^{2}
	61	5.43×10^{2}
	89	1.49×10^{3}
	119	4.17×10^{3}

Assuming that molecular oxygen adsorbs on an oxygen vacancy formed by the Sr incorporation, the σ should decrease by the following equilibrium (**1**): O_2 (g)$+2e^- = 2O^-$ (ads) where e^- is a conduction electron trapped at an oxygen vacancy, satifying the data in Figure 8. In equilibrium (**1**), the adsorbed oxygen dissociates into two oxygen species and their concentration increase with increasing P_{O_2}. The two oxygen species satisfy the half order with respect to oxygen

in accordance with the kinetic data. The data in Table 3 indicate that equilibrium (1) moves to the right, showing an oxygen vacancy defect is a possible site involved in adsorption of oxygen. The increasing σ with P_{CO} indicates that electron density increases with increasing CO adsorption. Assuming that a lattice oxygen is a possible site for CO adsorption, the σ should increase based on the following equilibrium (2) : CO (g)+O^{2-} (latt)=e^-+CO_2^- (ads) where CO_2^- (ads) is adsorbed carbon dioxide ion. The equilibrium (2) moves to the right with P_{CO} and as a result σ increases with electron density.

According to the kinetic data shown in Table 2, the following elementary reaction (3) should be involved in the total oxidation reaction, since the reaction rate increase with P_{CO} and P_{O_2} : (3) CO_2^- (ads)+O^-(ads)$\longrightarrow$$CO_2$ (g)+O^{2-} (latt). In order to test the inhibition effect of the product CO_2 and to know that the elementary reaction (3) is reversible or not, the product was not frozen out by liquid nitrogen. As a result, the first order with respect to $(P_{CO}+P_{O_2})$ was obtained, showing half orders for CO and O_2, respectively. This indicates that the product CO_2 inhibits the reaction rate and therefore, the elementary reaction (3) should be represented as following equilibrium (4) : CO_2^- (ads)+O^- (ads)=CO_2 (g) +O^{2-} (latt). From the kinetic data, it is known that the product CO_2 also adsorbs on catalyst surface. In equilibria (1), (2) and (4) and elementary reaction (3), the equilibrium constants and rate constant are designated as K_1, K_2, and K_4 and k, respectively.

Kinetics and Mechanisms. The reaction rate of CO_2 production can be represented as $d(CO_2)/dt=k(CO_2^-)(O^-)$ from the elementary reaction (3). This rate law can be written as $d(CO_2)/dt=kK_1^{1/2}K_2(CO)(O_2)^{1/2}$ with substitutions of $(CO_2^-)=K_2(O^{2-})(CO)/(e^-)$ from equilibrium (2) and $(O^-)=K_1^{1/2}(O_2)^{1/2}(e^-)$ from equilibrium (1), taking (O^{2-}) to be constant, consistent with experimental rate law $-dP/dt=k'P_{CO}P_{O_2}^{1/2}$ for $kK^{1/2}K_2=k'$. Under the CO_2 inhibition, however, the rate law should be represented as $d(CO_2)/dt=k(\theta_{CO}/\theta_{CO_2})(\theta_{O_2})$ where θ_{CO}, θ_{CO_2} and θ_{O_2} are all surface coverages of CO, CO_2 and O_2 molecules, respectively. $d(CO_2)/dt=k(bP_{CO}/1+bP_{CO})/(bP_{CO_2}/1+bP_{CO_2})\times(b^{1/2}P_{O_2}^{1/2}/1+b^{1/2}P_{O_2}^{1/2})$ with the Langmuir's ideal adsorption and b the adsorption coefficient. The concentration of oxygen vacancy is very low, namely $\theta_{O_2}<1$ and if the equilibrium (1) is a rate controlling step, one can obtain $d(CO_2)/dt=(kb_{CO}b_{O_2}^{1/2})/(b_{CO_2})(P_{CO}/P_{CO_2})P_{O_2}^{1/2}=k'(P_{CO}/P_{CO_2})P_{O_2}^{1/2}$, showing first order kinetics; half orders with respect to CO and O_2, respectively. The kinetic data agree well with the above rate law with $\alpha=0.5$ without a CO_2 trap. Also, the kinetic data agree well with $\alpha=1$ and a CO_2 trap.

Concludingly, the reaction mechanisms follow the equilibria (1), (2), and (4), and elementary reaction (3) on the basis of our experimental results that the oxygen vacancy formation due to Sr substitution is the important role for the CO oxidation on $Eu_{1-x}Sr_xCoO_{3-y}$ catalysts and the catalytic activity would be related to electrical properties. In this case, the catalytic activity is enhanced by Sr doping up to $x=0.5$ in spite of the space charge.

Acknowledgement. We are grateful to the Ministry of Science and Technology of Korea for the financial support and to Dr. T.J. Kim for helpful advices. We thank also Dr. S.K. Cho for the assistance of the various measurements.

References

1. J. S. Choi, K. H. Kim, and S. R. Choi, *Int. J. Chem. Kinet,* **9**, 489 (1977).
2. H. Chon and C. D. Prater, Discuss, Faraday Soc., **41**, 380 (1966).
3. B. M. Arghiropoulos and S. T. Teichner, *J. Catal.,* **3**, 477 (1964).
4. J. H. Boer, "Reactivity of Solids", p. 381, Elsevier, Amsterdam, 1961.
5. K. H. Kim, H. S. Han, and J. S. Choi, *J. Phys. Chem.,* **83**, 1286 (1979).
6. K. H. Kim and J. S. Choi, *J. Phys. Chem.,* **85**, 2447 (1981).
7. K. H. Kim, S. H. Lee, Y. R. Kim, and J. S. Choi, *J. Catal.,* **88**, 283 (1984).
8. S. H. Lee, G. Heo, K. H. Kim, and J. S. Choi, *Int. J. Chem. Kinet.* **19**, 1 (1987).
9. K. H. Kim, D. Kim and J. S. Choi, *J. Catal.,* **86**, 219 (1984).
10. R. J. H. Voorhoeve, "Advanced Materials in Catalysis", p. 129. Academic Press, New York, 1987.
11. E. K. Cho, W. Y. Chung, K. H. Kim, K. M. Choi, and J. S. Choi, *J. Am. Ceram. Soc.* **73**, 3470 (1990).
12. K. H. Kim, D. Y. Yim, K. M. Choi, J. S. Choi, and R. G. Sauer, *J. Phys. Chem. Solids,* **50**, 1027 (1989).
13. J. S. Park, K. M. Choi, K. H. Kim, and J. S. Choi, *J. Phys. Chem. Solids,* **50**, 909 (1989).
14. D. Kim, K. M. Choi, K. H. Kim, and J. S. Choi, *J. Phys. Chem. Solids,* **50**, 821 (1989).
15. K. M. Choi, K. H. Kim, and J. S. Choi, *J. Phys. Chem. Solids,* **49**, 1027 (1988).
16. K. H. Kim, D. Y. Yim, S. H. Park, and J. S. Choi, *J. Phys. Chem. Solids,* **49**, 151 (1988).
17. H. J. Won, S. H. Park, K. H. Kim, and J. S. Choi, *J. Phys. Chem. Solids,* **48**, 383 (1987).
18. J. S. Choi, H. Y. Lee, and K. H. Kim, *J. Phys. Chem.,* **77**, 2430 (1973).
19. J. S. Choi, Y. H. Kang, and K. H. Kim, *J. Phys. Chem.,* **81**, 2208 (1977).
20. K. H. Kim and J. S. Choi, *J. Phys. Chem.,* **85**, 2447 (1981).
21. K. H. Kim, S. H. Lee, G. Heo, and J. S. Choi, *J. Phys. Chem. Solids,* **48**, 895 (1987).
22. K. M. Choi, K. H. Kim, and J. S. Choi, *J. Phys. Chem.* **93**, 4659 (1989).
23. McIlvried McCarthy, *JCPDS,* **25**(1054), (1973).
24. I. Shaplygin and V. Lazarev, *JCPDS,* **38**(1148), (1985).
25. L. V. Azaroft and M. J. Buerger, "The Powder Method in X-ray Crystallography", pp. 239-245, McGraw-Hill, 1958.
26. D. W. Strickler and W. G. Carlson, *J. Am. Ceram. Soc.,* **47**, 122 (1964).